Am J Clin Exp Urol 2019;7(3):139-152
www.ajceu.us /ISSN:2330-1910/AJCEU0097329

Original Article

Carcinogen-induced bladder cancer in the FVB mouse strain is associated with glandular differentiation and increased Cd274/Pdl-1 expression

Vasty Osei Amponsa[1], Lauren Shuman[1], Justine Ellis[1], Erica Wang[1,2], Vonn Walter[2,4], Russell G Owens[1,2], Michael Zaleski[1], Joshua I Warrick[1], Jay D Raman[4], David J DeGraff[1,3,4]

[1]Department of Pathology, Pennsylvania State University College of Medicine, Hershey, PA, USA; Departments of [2]Public Health Sciences, [3]Biochemistry and Molecular Biology, Pennsylvania State University College of Medicine, Hershey, PA, USA; [4]Division of Urology, Department of Surgery, Pennsylvania State University College of Medicine, Hershey, PA, USA

Received May 21, 2019; Accepted May 30, 2019; Epub June 15, 2019; Published June 30, 2019

Abstract: Background: Creation of genetically engineered mouse models of bladder cancer often involves the use of several background strains in conjunction with the carcinogen N-butyl-N-(4-hydroxybutyl) nitrosamine (BBN). However, carcinogen susceptibility in commonly used strains, as well as phenotypic differences is not well characterized. Objectives: To determine differences in susceptibility and phenotypic outcome following BBN exposure of C57BL/6 and FVB, two strains commonly used for model development. Methods: Male C57BL/6 and FVB mice were exposed to BBN (0.05%) in drinking water for 12 and 16 weeks. Dissected bladders were characterized by histological and immunohistochemical analyses. Gene Ontology analysis was performed to identify differences in gene expression across strains following BBN exposure. Results: While the C57BL/6 strain developed non-invasive tumors, FVB mice developed muscle invasive bladder cancer with squamous and/or glandular differentiation. Glandular differentiation was exclusively observed in the FVB strain. FVB tumors were highly immunogenic and inflamed by the presence of high expression of Cd274 (Pdl-1), murine histocompatibility complex (H2) and pro-inflammatory cytokines (Il-5 and Il-17). Conclusions: Following BBN exposure, FVB mice undergo rapid tumorigenesis and disease progression characterized by Pdl-1 expression and development of glandular differentiation. These studies identify a degree of tumor heterogeneity in the FVB tumors previously undescribed, and identify FVB mice as a potentially useful model for the study of bladder adenocarcinoma and the inflammatory tumor microenvironment.

Keywords: PDL-1, immune checkpoint, strain, bladder cancer, glandular differentiation, BBN N-butyl-N-(4-hydroxybutyl) nitrosamine, carcinogen

Introduction

Bladder cancer is the second most common genitourinary malignancy in the United States with an estimated 81,190 new diagnoses and 17,340 deaths in 2018 [1]. At clinical presentation, approximately 60-70% of bladder cancer patients are diagnosed with non-muscle invasive bladder cancer (NMIBC) while the remaining 30-40% of patients present with muscle invasive bladder cancer (MIBC) with or without metastasis [2]. In addition to the need for accurate tumor staging, development of a treatment strategy for bladder cancer is driven by several factors including the histopatological features of the tumor. Approximately 90% of bladder cancer cases are diagnosed primarily as urothelial cell carcinoma (UCC) while an additional 5% are identified as squamous cell carcinoma (SCC). The remainder of diagnoses includes other relatively rare pure histologic variants such as adenocarcinoma, plasmacytoid variant, small cell carcinoma, and other variants [3]. In addition to these pure histologic subtypes, variant histology is often present in a manner that is admixed with UCC. For example, up to 40% of UCC exhibits elements of squamous differentiation (SqD) or other morphologic variant patterns. Recent studies show that morphologic variants of bladder cancer are associated with unique gene expression patterns and phenotypic behavior [4]. As the presence of

morphologic variation is associated with differences in response to therapy [5], increased efforts are required to understand the impact of tumor heterogeneity on disease progression and clinical outcomes.

The use of carcinogen-based models of malignant disease has significantly advanced our understanding of the biologic processes underlying disease pathogenesis and tumor progression. Because of the lack of *in vivo* model systems that effectively recapitulate the heterogeneity (morphology, genomic alterations, metastatic capacity) in human pathologic disease, preclinical models often fail in the identification of therapeutic approaches that exhibit clinical effectiveness in humans [6, 7]. As there are relatively limited *in vivo* models in bladder cancer research [8-10], the establishment of improved models suitable for therapeutic assessment is essential.

Exposure of rodents to the chemical N-butyl-N-(4-hydroxybutyl) nitrosamine (BBN) is widely used as a preclinical model for the study of bladder cancer [9, 11-13]. A derivative of the environmental carcinogen N-nitrosodi-n-butylamine, BBN is also a metabolite derived from a N-nitroso compound present in tobacco, which is a major risk factor for bladder cancer development in western countries. Oxidation of BBN in the liver generates *N*-n-butyl-*N*-(3-carboxypropyl) nitrosamine (BCPN) metabolite, which, in addition to BBN, is considered to be the driving factor for bladder tumorigenesis [14-16]. Because of these reasons and the organ-specific mutagenicity of BBN [17], the BBN-induced carcinogenesis model is particularly effective for assessing the impact of environmental carcinogen exposure on bladder cancer development.

Several studies have shown that BBN-induced bladder tumors exhibit species and strain-specific phenotypes [18-21]. For example, while administration of BBN to Wistar rats for 10 weeks results in the development of non-invasive superficial papillary bladder carcinoma, 10 weeks of BBN exposure in the BABL/C mouse strain results in the development of invasive bladder carcinoma [22]. In addition, it has been shown that strain differences within a species correlate with sensitivity to BBN-induced bladder carcinogenesis resulting in different histopathologic phenotypes [23-26]. These findings are in agreement with extensive documentation regarding differential strain susceptibility in other preclinical animal systems [27, 28].

While all preclinical models have limitations, BBN treatment does result in reproducible neoplastic changes in the murine urothelium. For this reason, BBN is additionally used in conjunction with genetically engineered (transgenic and knockout) mouse models to test hypotheses regarding the interplay between environmental carcinogens and underlying genetic alterations. Nonetheless, the generation of genetically engineered mouse models often involves breeding schemes that incorporate different strains; therefore, it is crucial to understand the extent to which common mouse strains used in the creation of genetically engineered mouse models are susceptible to BBN-induced bladder cancer. Therefore, as a foundational study, we performed experiments to determine the degree to which, if any, two of the most commonly used mouse strains, C57BL/6 and FVB, exhibit differential susceptibility to BBN carcinogen.

Materials and methods

Animals

All animal studies were approved by Institutional Animal Care and Use Committee of Pennsylvania State University College of Medicine (PSCOM). Adult male C57BL/6 and FVB mice were purchased from The Jackson Laboratory (Bar Harbor, ME) and were housed within the PSUCOM animal facility with 12 hours regulated day/night cycle at 68-73°F room temperature. Mice were fed with rodent diet (2016 Teklad global 16% protein rodent diets, Madison WI), and water *ad libitum*.

Carcinogen treatment

The chemical N-butyl-N-(4-hydroxybutyl) nitrosamine (BBN; TCI America; Portland OR) was prepared at 0.05% solution in water and administered *ad libitum* in drinking water. Mouse drinking water was changed twice per week, and water bottles were covered with aluminum foil to prevent light exposure. 8 weeks old mice were exposed to BBN for 12 weeks (C57BL/6, n = 18 and FVB, n = 20), for 16 weeks (C57BL/6, n = 8 and FVB, n = 12) and for 20 weeks (C57BL/6, n = 5). Because FVB mice were mori-

bund after 16 weeks of BBN exposure, we did not expose these mice to further BBN treatment. At the specified time points, BBN treatment was discontinued, and mice were exposed to normal water *ad libitum* for one week before euthanized via isoflurane (Vedco; Saint Joseph MO) inhalation followed by cervical dislocation. Bladders were then dissected and fixed in 10% neutral-buffered formalin (VWR International; Radnor PA) and subsequently stored in 70% ethanol (Pharmaco-Aaper; Brookefield CT) prior to processing and paraffin embedding. A total of 6 mice (C57BL/6, n = 3 and FVB, n = 3) and a total of 9 (C57BL/6, n = 4 and FVB, n = 5) from the 12-weeks-BBN treated group were used for RNA-sequencing (RNA-seq) and Western blot respectively.

Histology and immunohistochemistry

Tissue sections were deparaffinized and used for H&E staining and immunohistochemistry (IHC) as previously reported [29]. One C57BL/6 mouse treated for 12 weeks with BBN was excluded for further characterization because of the inability to define the histologic type due to small bladder size. For IHC, slides were deparaffinized in histoclear (National Diagnostics; Atlanta GA), rehydrated in a series of graded alcohols (Pharmaco-Aaper; Brookefield CT) and washed in deionized water. The slides were placed in 1% antigen unmasking solution (Vector Labs; Burlingame CA) and heated for 20 minutes at high pressure in a pressure cooker (Cuisinart; East Windsor NJ), followed by cooling at room temperature and 10 minutes washes in phosphate-buffered saline (PBS 1X, pH 7.4) for 3 times. Incubation in 1% hydrogen peroxide (Thermo Fisher Scientific; Fremont CA) in methanol (Thermo Fisher Scientific) for 20 minutes was performed to block endogenous peroxidase activity. Slides were rewashed in 1X PBS (10 minutes for 3 times) and incubated for 1 hour in blocking solution 1X PBS containing horse serum (Vector Labs) to reduce nonspecific antibody binding. Subsequently, slides were incubated with primary antibodies overnight at 4°C in a humidified chamber. Antibodies used were diluted in blocking solution and included goat polyclonal anti-FOXA1 (1:1000; Santa Cruz Biotechnology, Santa Cruz CA; #sc-6553), rabbit monoclonal anti-Ki67 (1:1000; Abcam, Cambridge MA; #ab16667), mouse monoclonal anti-KRT5/6 (1:200; Dako, Santa Clara, CA; #D5/16 B4), mouse monoclonal anti-KRT14 (1:200; Novocastra Leica Biosystem, Buffalo Grove IL; #LL002-L-CE), rabbit polyclonal anti-PPARG (1:200; Cell Signaling; #2430S), rabbit polyclonal anti-CDX2 (1:50; Sigma; #HPA049580). Mouse intestine was used as a positive control for CDX2 IHC.

The following day, slides were washed in 1X PBS (10 minutes for 3 times) before incubation for 1 hour with appropriate secondary antibody (1:200; Vector Labs) diluted in blocking solution. Following additional washing, antibody binding was visualized through the Vectastain Elite ABC Peroxidase kit (Vector Labs) after addition of the chromogen 3'-diaminobenzidine (Dako). Sections were washed in tap water for 5 minutes before counterstaining and rehydration as previously reported [29]. To reduce potential background noise and cross-reaction on mouse tissues, the mouse on mouse kit (Vector Labs) was used for IHC staining performed with antibodies raised in mouse. For IHC quantification, percent cells positive for Foxa1 were multiplied by staining intensity (graded 0-3) to calculate H score and percent positive cells were used for Pparg, Krt5/6, Krt14, and Ki67 staining.

For morphologic characterization of the bladder tumors, the following rules were applied: variant morphology was defined as anything other than conventional UCC identified via H&E examination. Specimens with hyperplasia and nuclear atypia in the urothelial lining in the absence of observable invasion were classified either flat urothelial carcinoma *in situ* (CIS) or CIS with keratinizing squamous metaplasia (KSM) in the presence of squamous changes. However, bladder tissues exhibiting squamous elements in the setting of tumor invasion were referred to as squamous differentiation (SqD), and tumors showing glandular differentiation (GD) in the presence of additional variant morphology were considered glandular. When multiple tumor morphologies/stages were present (i.e., CIS, pTa disease or frank invasion, for example), the tumor was designated as the highest stage present. All tumor staging, morphologic characterization, and quantification of IHC were performed in a blinded manner by genitourinary pathologists (JIW and MZ).

RNA-sequencing and computational analysis

In an effort to identify differences in gene expression between strains following BBN

exposure, bladders were dissected from C57BL/6 (n = 3) and FVB mice (n = 3) after 12 weeks of BBN exposure and stored in RNAlater solution (Thermo Fisher Scientific) to stabilize RNA. Extraction of RNA was performed using TriZol (Thermo Fisher Scientific) reagent according to the manufacturer's instructions. One sample from the C57BL/6 mice was omitted for further analysis because of RNA degradation. RNA-seq was performed by the Genome Sciences and Bioinformatics Facility at the Pennsylvania State College of Medicine. The RNA-seq data were normalized to fragments per kilobase of transcript per million (FPKM) and used for differential expression analysis through the limma package [30] and R Commander software version 3.3.1 [31]. Differentially expressed genes between the strains were identified using a false discovery rate threshold of q = 0.05. Gene Ontology (GO) analyses were performed using the Database for Annotation, Visualization and Integrated Discovery (DAVID) [32, 33]. Genes differentially expressed in the two strains with q < 0.05 (Tables S1 and S2) were uploaded on DAVID and analyzed on *Mus musculus* species background using the default annotation categories as defined by DAVID. A medium classification stringency was chosen for DAVID functional annotation clustering analyses, based on which, groups of terms/annotations sharing similar gene members with similar biological meaning are clustered together. For this study, we focused on the GO biological process annotations to identify pathways modulated in FVB versus C57BL/6 following BBN exposure. Genes associated with the identified biological processes were used to generate gene expression heatmaps in which the expression values are median centered by gene.

Western blot

A total of 9 dissected mouse bladders were homogenized in radioimmunoprecipitation (RIPA) buffer (25 mM Tris-HCl pH 7.6, 150 mM NaCl, 1% NP-40, 1% sodium deoxycholate, 0.1% SDS) (Thermo Scientific, #89901) containing 1X protease inhibitors (Roche, #11697498001), 1X phosphatase inhibitors (Roche, #4906837001) and 1 nM Dithiothreitol (DTT) (Invitrogen) in microcentrifuge tubes with a pestle (USA Scientific, #1415-5390). The homogenized tissues were left on ice for 30 minutes for the lysis process and then sonicated 4 seconds (x^2) before spinning at 15,000xg for 30 minutes at 4°C. Protein concentrations were measured by optical densitometry at 562 nm wavelength using Pierce BCA Protein Assay Kit (Thermo Scientific; #23225) according to the manufacturer's protocol. Lysate samples were prepared with 1X NuPAGE LDS Sample buffer (Thermo Scientific; #NP0007) at 1 µg/ml final concentration. Samples were boiled at 95°C for 5 minutes to reduce and denature proteins. A total of 10 µg of proteins per sample was loaded on polyacrylamide gel (Thermo Scientific; #NP0323BOX) together with protein marker (BioRad; #1610374) for electrophoresis at 85-90 Volts power (BioRad) followed by blotting on PVDF membrane equilibrated first in 100% methanol, washed with Millipore water and then re-equilibrated with transfer buffer (Thermo Scientific; #NP0006-1). Blotting was performed using Pierce G2 Fast Blotter (Thermo Scientific) at 25 Volts power for 15 minutes. Membranes were incubated in blocking buffer (5% skim milk - Tris-buffered saline (BioRad; #170-6435) containing 0.1% Tween20 (Thermo Scientific; #BP337-500; TBST) for 1 hour at room temperature on a shaker to block unspecific antigens. Membranes were incubated with primary antibodies overnight at 4°C. Primary antibodies used were diluted in blocking buffer: goat polyclonal anti-PDL-1 (1:400; R&D Systems; #AF1019), rabbit monoclonal anti-CD80 (1:1000; Abcam; #ab134120), rabbit monoclonal anti-CD86 (1:5000; Abcam; #ab53004) and rabbit anti-PPARG (1:1000; Cell Signaling Technology; #2430). On the next day, membranes were washed in TBST 3 times 10 minutes each before incubation with secondary antibody (anti-goat or anti-rabbit; 1:2000) for 1 hour at room temperature on a shaker. Membranes were rewashed in TBST 3 times 10 minutes each followed by treatment with Amersham ECL Prime Western Blotting Detection Reagent (GE Healthcare Life Sciences, #RPN2232) for visualization of protein bands. Image J software was used to quantify protein bands.

Statistical analysis

The Wilcoxon rank sum test was used to identify significant differences in strain-specific bladder weights, IHC scores and protein levels of Pdl-1 expression upon BBN exposure. One FVB mouse was omitted as an outlier for the

statistical analysis of Pdl-1 expression in the strains. Following dichotomization to compare non-invasive (hyperplasia and pTa) to invasive (pT1 or greater) disease, Fisher's exact test was used to identify significant associations between mouse strain and tumor invasion following BBN exposure. Two-Sided exact Cochran-Mantel-Haenszel test was applied for analysis of the association between strain background and histologic differentiation. The mouse tumors were stratified by stage (pTa/pTis/pT1 versus pT2/pT3) and analyzed using a 2x2 table for the association between strain and glandular differentiation. *P*-values ≤ 0.05 were considered statistically significant. Prism version 6.0c (GraphPad Software) was used for Wilcoxon rank sum test; and R Commander software for Fisher's exact test.

Results

FVB mice exhibit rapid bladder tumorigenesis and disease progression following BBN exposure

Following 12 weeks of BBN exposure, bladders dissected from FVB mice were significantly heavier when compared with bladders dissected from C57BL/6 mice (**Figure 1A**; FVB median = 80 mg versus C57BL/6 median = 45 mg; *p*-value = 0.0393, Wilcoxon rank sum test). The FVB bladders trended on being heavier than C57BL/6 bladders following 16 weeks of BBN exposure, but differences were not statistically significant (**Figure 1B**). The observed tumor stage in C57BL/6 following 12 weeks of BBN exposure was predominantly urothelial pTis (CIS 100%) (**Figure 1C**). Although pTis stage disease persisted, progression to pT1 stage disease was noted in approximately 38% of C57BL/6 mice after 16 weeks on BBN (**Figure 1C**). As previously reported [34], prolonged BBN exposure for 20 weeks led to further tumor invasion into the muscularis propria (pT2) and perivesical fat (pT3) in C57BL/6 (Figure S1A). Conversely, pT3 disease (invasion through the muscle into perivesical fat) was the most commonly observed tumor stage phenotype in FVB following 12 weeks (~42%) and 16 weeks (~58%) of BBN exposure (**Figure 1C**). We identified co-occurrence of pTa and pTis lesions in a number of C57BL/6 mice after 12 weeks (n = 3) and 16 weeks (n = 4) of BBN treatment. After 16 weeks of BBN exposure, we also identified concomitant presence of pTa and pT1 disease (n = 1), and pTis and pT1 lesions (n = 1) in C57BL/6 mice. Multiple lesion types were also detected in FVB mice. Following 12 weeks of BBN exposure, we observed concomitant pTa and pTis disease (n = 1) as well as co-occurrence of pTis and pT1 (n = 1), and pTis and pT3 (n = 1). After 16 weeks of BBN exposure, one FVB mouse had both pTa and pT1 disease, and another FVB mouse had pTis and pT1 disease.

Examples of normal urothelium (non-exposed bladder; **Figure 1D**), urothelial hyperplasia, CIS and non-invasive papillary tumors complete with a well-developed fibrovascular core in C57BL/6 are shown (**Figure 1E-J**). In addition, we provide examples of normal urothelium (**Figure 1K**), lamina propria invasion (**Figure 1L**, **1M**). Statistical analysis shows that FVB mice were significantly more likely to develop invasive bladder cancer (tumor stage ≥ pT1) following 12 weeks of BBN exposure compared with C57BL/6 mice ($p = 0.013$, Fisher's exact test); however, these differences were not significant after 16 weeks of BBN exposure as C57BL/6 mice develop invasive disease from this time point.

In summary, both C57BL/6 and FVB mice exhibit multiple lesions of various stages following BBN exposure. Our data show that FVB mice develop tumors rapidly and display a significantly increased likelihood of tumor invasion at an earlier time point relative to C57BL/6 when exposed to BBN.

Glandular differentiation is enriched in FVB strain bladder tumors following BBN exposure

As tumor heterogeneity is reported to have prognostic significance, and bladder cancer is a highly heterogeneous disease exhibiting different response to therapy [5, 35], we next sought to define the degree of tumor heterogeneity in C57BL/6 and FVB mice following BBN-induced carcinogenesis. While FVB mice exhibited rapid tumorigenesis and disease progression in comparison to C57BL/6, the histological differences between FVB and C57BL/6 mice were also striking. Overall, C57BL/6 mice developed dramatic urothelial atypia interpreted as non-invasive flat UCC with squamous features after 12 weeks (~37%) and 16 weeks (~50%) of BBN exposure (**Figure 2A**). Histological variants consisted of KSM complete with the presence of intercellular bridging and keratin deposition (**Figure 2B-G**), and these findings are consistent with a recent report indicating C57BL/6

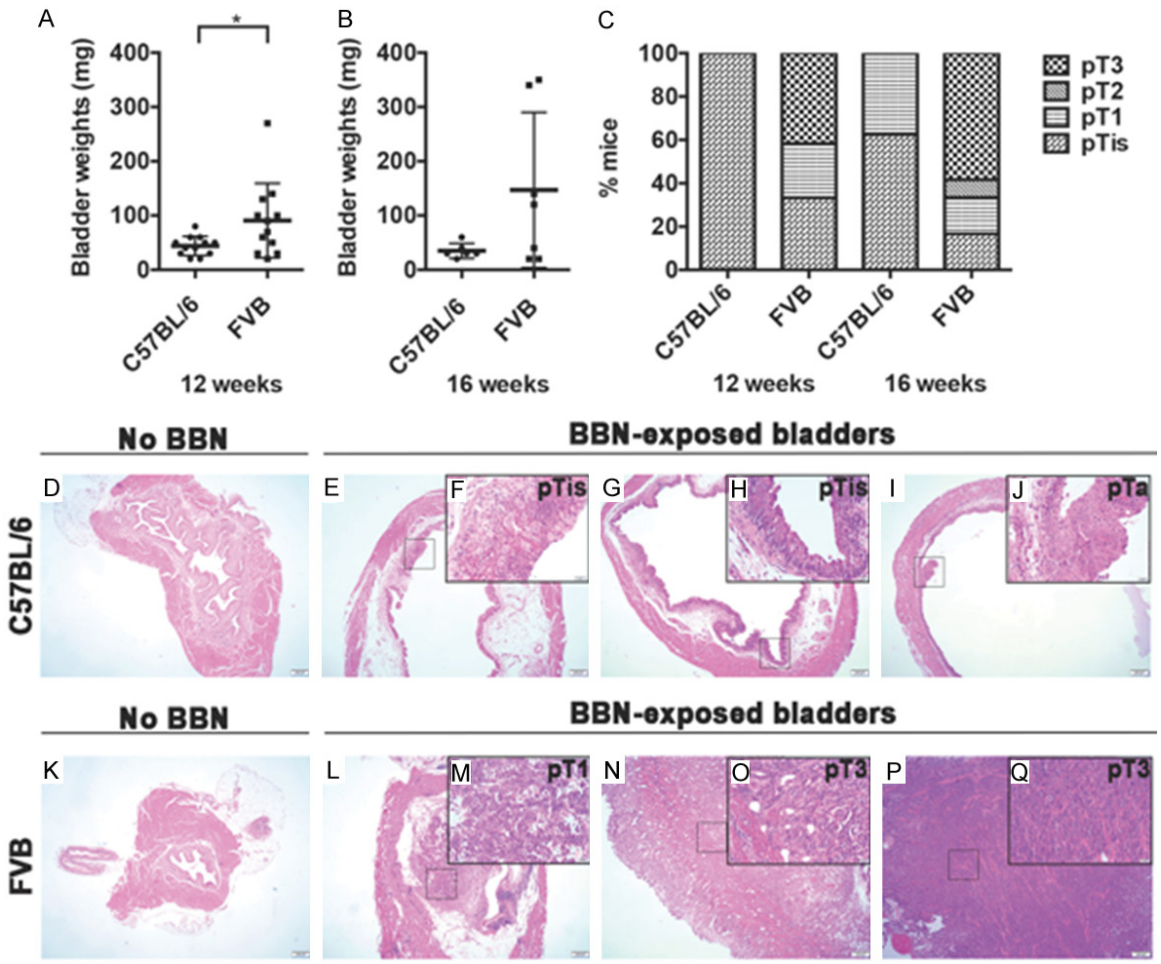

Figure 1. FVB strain of mice develops more advanced stage bladder cancer compared with C57BL/6 following BBN exposure. (A, B) The weights of bladders dissected from C57BL/6 and FVB mice following (A) 12 weeks and (B) 16 weeks of BBN exposure are shown. Each dot represents one animal. After 12 weeks of BBN exposure, the bladders of FVB mice were significantly heavier than the bladders from C57BL/6 mice (*p-value = 0.0393; Wilcoxon rank sum test). Differences in bladder weights following 16 weeks of treatment were not statistically significant (p-value = 0.2442; Wilcoxon rank sum test). (C) Percentage of C57BL/6 and FVB mice with a given tumor stage. Following 12 weeks on BBN, C57BL/6 (n =11) developed pTis (n = 11) disease whereas FVB (n = 12) developed pTis (n = 4), pT1 (n = 3) and pT3 (n = 5) disease. After 16 weeks on BBN, C57BL/6 (n = 8) developed pTis (n = 5) and pT1 (n = 3) disease whereas FVB (n = 12) developed pTis (n = 2), pT1 (n = 2), pT2 (n = 1) and pT3 (n = 7) disease. (D-Q) H&E sections of non-exposed and BBN-exposed bladders dissected from C57BL/6 (D-J) and FVB (K-Q) mice. Image scale bar 200 μm (low power magnification) and inset with higher magnification scale bar: 50 μm.

mice exposed to BBN develop basal bladder cancer [36], which is often enriched with SqD in humans [37]. Conversely, FVB mice exhibited more morphologically heterogeneous disease seen as UCC admixed with invasive SqD and GD (**Figure 2H-M**), both of which were respectively present at a frequency of ~25% and ~17% after 12 weeks of BBN, and each at a frequency of ~33% after 16 weeks of BBN exposure (**Figure 2A**). While FVB mice developed GD and SqD following BBN exposure, we detected no GD in C57BL/6 mice after 12 and 16 weeks (**Figure 2A**) or after prolonged exposure (Figure S1B-S1D). When we accounted for tumor stage, we did not observe a significant association between strain and glandular differentiation (p-value = 0.11, two-sided exact Cochran-Mantel-Haenszel test) suggesting advanced tumor stage may increase the likelihood of GD phenotype, independent of strain background. However, while advanced stage disease (pT3) in C57BL/6 at 20 weeks of BBN were associated with SqD, no GD phenotype was detected at this time point in C57BL/6 mice. Therefore, these data suggest that while FVB mice develop advanced stage bladder tumors with elements of UCC, SqD, and GD as early as at 12 weeks of BBN exposure, C57BL/6 mice devel-

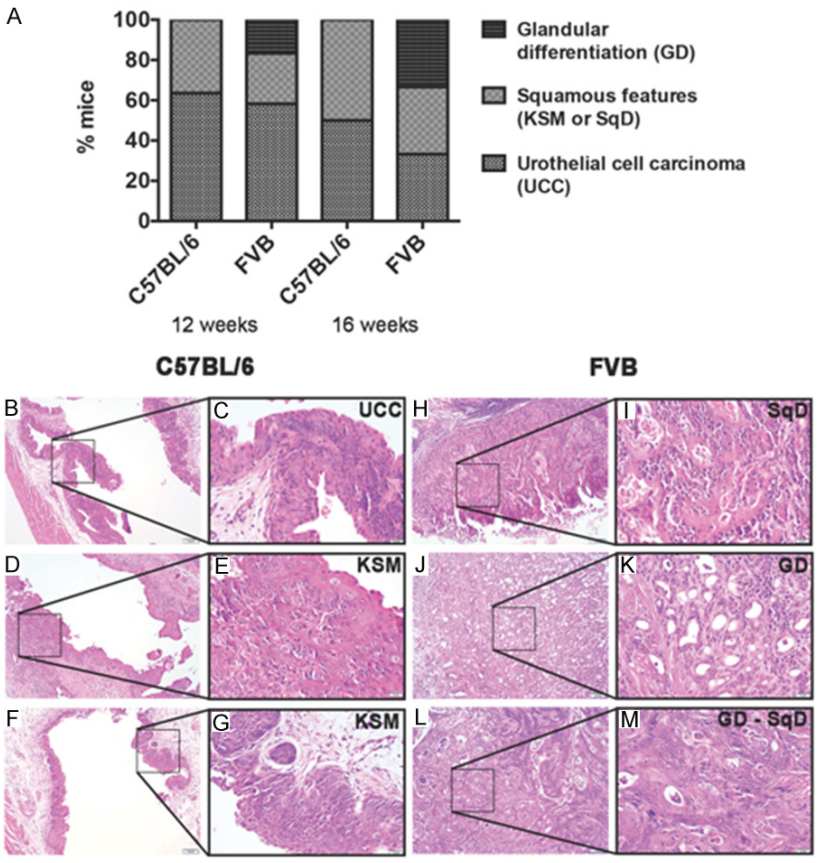

Figure 2. FVB mice exhibit squamous and glandular morphologic variants of urothelial carcinoma in response to BBN. (A) Percentage of C57BL/6 and FVB mice with urothelial cell carcinoma (UCC), squamous features [keratinizing squamous metaplasia (KSM) or squamous differentiation (SqD)] and glandular differentiation (GD) following 12 and 16 weeks of BBN treatment. (B-M) H&E sections of bladders tissue dissected from C57BL/6 (B-G) and FVB (H-M) mice exposed to BBN for 12 and 16 weeks. Morphologic assessment of C57BL/6 bladders revealed non-invasive flat UCC (B, C, 12 weeks of BBN exposure) or KSM (D, E, 12 weeks of BBN exposure; and F, G, 16 weeks of BBN exposure) characterized by intracellular bridging and keratin deposition. Morphologic assessment of FVB bladders revealed invasive UCC with the presence of SqD (H, I, 12 weeks of BBN exposure) or GD (J, K, 12 weeks of BBN exposure) as well as mixed GD with SqD (L, M; 16 weeks of BBN exposure). Image scale bar 100 μm (low power magnification) and inset with higher magnification scale bar 20 μm.

op invasive tumors with elements of UCC and SqD at late time points such as 16 weeks and 20 weeks of carcinogen exposure (Figure S1).

Immunohistochemical analysis confirms strain-dependent influence of BBN treatment on tumor morphology

Specific morphologic variants are associated with the expression of immunohistochemical markers indicative of differentiation state. For example, while expression of high molecular weight cytokeratins including Krt5/6 and Krt14 is associated with squamous morphology [38], expression of the transcriptional regulators, peroxisome proliferator-activated receptor gamma (Pparg) and Forkhead box A1 (Foxa1) is associated with urothelial and glandular differentiation [38]. Therefore, we next explored the expression of these markers in the tumors of our experimental mice. While C57BL/6 mice exhibited moderate to high expression of Krt5 and Krt14 in their BBN-induced tumors, they exhibited mild and often undetectable nuclear Pparg or Foxa1 expression in these tumors (**Figure 3A**). On the other hand, as BBN-associated tumors in FVB mice were characterized by SqD and GD, we observed high expression of both squamous markers (Krt5 and Krt14) and the urothelial marker (Foxa1) whereas Pparg expression was low (**Figure 3A**). Scoring of IHC showed no significant difference between C57BL/6 and FVB tumors regarding the levels of expression of Krt5 (**Figure 3B**) and Krt14 (**Figure 3C**). However, the IHC scoring also showed that Pparg levels were significantly lower in FVB tumors compared with C57BL/6 tumors (**Figure 3D**) whereas Foxa1 levels were significantly higher in FVB tumors relative to C57BL/6 tumors (**Figure 3E**). Altogether, these findings are suggestive of the existence of divergent morphologic patterns in C57BL/6 and FVB mice following BBN exposure.

C57BL/6 and FVB mice exhibit differential expression of Cd274 (Pdl-1) in tumor bladders following BBN exposure

In order to develop a more in-depth understanding of the molecular differences that

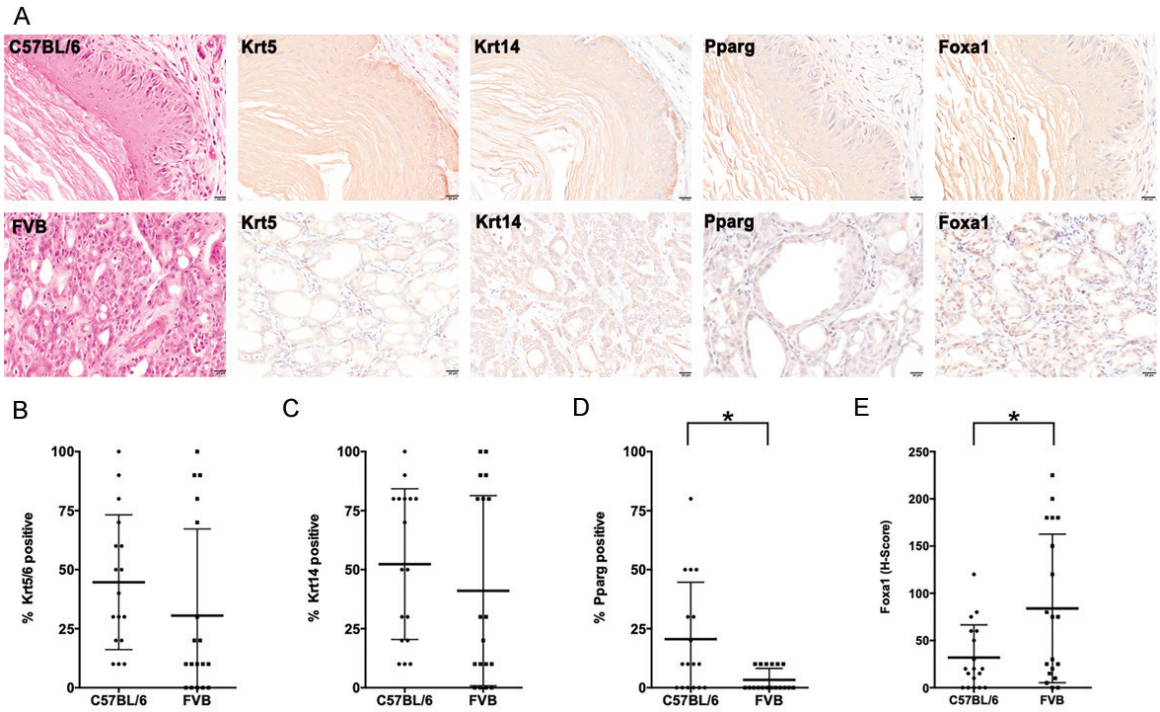

Figure 3. Immunohistochemical analysis suggests divergent differentiation patterns in BBN-induced bladder cancers in C57BL/6 and FVB mice. (A) H&E staining and immunohistochemistry (IHC) for Krt5/6, Krt14, Pparg, and Foxa1 in C57BL/6 and FVB mice following 12 and 16 weeks of BBN exposure. (B, C) Tumors from FVB and C57BL/6 mice did not express significantly different levels of the basal markers, (B) Krt5 and (C) Krt14; each dot represents a mouse. (D, E) Quantification of IHC for Pparg and Foxa1, both associated with urothelial differentiation, revealed significantly lower expression of (D) Pparg, but higher expression of (E) Foxa1 in FVB mice (* = $P \leq 0.05$; Wilcoxon rank sum test). Each dot represents a mouse.

underlie the non-invasive tumors in C57BL/6 mice versus the invasive tumors in FVB mice, we performed RNA-seq on dissected bladders after 12 weeks of BBN exposure followed by differential expression analysis (see Tables S1 and S2) and subsequent functional annotation studies using the NIH DAVID software. We found that upregulated genes in FVB mice relative to C57BL/6 mice were associated with GO terms related to the immune activity. Specifically, the FVB strain exhibited increased expression of genes related to the following biological processes: antigen processing and presentation via major histocompatibility complex (MHC/H2), immune response and proteolysis (**Tables 1** and S3 for clustering of functional annotations enriched in FVB). In contrast, genes differentially downregulated in FVB, but upregulated in C57BL/6 mice were involved in biological processes such as transport and GPCR signaling pathways (**Tables 1** and S4 for clustering of functional annotations enriched in C57BL/6). Based on this analysis indicating important differences in the tumor microenvironment, we further examined the differential expression between C57BL/6 and FVB strains for immune markers that are associated with cancer progression. Interestingly, we found evidence that immune markers including matrix metalloprotease (Mmp2 and Mmp9), interleukins and their receptors (Il-5, Il-5ra, Il-5rb, Il-6ra, Il-17b, Il-17ra and Il-17rb) as well as immune checkpoints (Cd274, Cd80 and Cd86) are upre-gulated in FVB mice relatively to C57BL/6 mice after 12 weeks of BBN exposure (**Figure 4A**); this suggests the presence of inflammation and ongoing immune reactivity in the FVB bladder tumors. Moreover, Pparg, which is known to be associated with immune suppression activity in the bladder tumor microenvironment [39], appeared to be upregulated in C57BL/6 mice compared to FVB mice at the RNA level (**Figure 4A**) supporting our IHC analysis (**Figure 3D**).

Table 1. List of genes differentially expressed in FVB mice versus C57BL/6 ranked by biologic process GO terms following DAVID analysis (Complete gene list found in Table S1)

Upregulated Genes in FVB versus C57BL/6		Downregulated Genes in FVB versus C57BL/6	
Gene Name	Gene Symbol	Gene Name	Gene Symbol
Immune response		Transport	
Histocompatibility 2, class II antigen E alpha, pseudogene	*H2-Ea-ps*	Afamin	*Afm*
Histocompatibility 2, Q region locus 1	*H2-Q1*	Apolipoprotein A-II	*Apoa2*
Histocompatibility 2, Q region locus 10	*H2-Q10*	Coiled-coil domain containing 109B	*Ccdc109b*
Histocompatibility 2, Q region locus 2	*H2-Q2*	Gamma-aminobutyric acid (GABA) A receptor, subunit alpha 3	*Gabra3*
Histocompatibility 2, T region locus 3	*H2-T3*		
Predicted gene 8909	*Gm8909*		
Proteolysis		GPCR signaling pathways	
Abhydrolase domain containing 1	*Abhd1*	Olfactory receptor 1034 (Olfr1034)	*Olfr1034*
Complement component 1, r subcomponent B	*C1rb*	Selection and upkeep of intraepithelial T cells 4	*Skint4*
Complement component 1, s subcomponent 2	*C1s2*	Selection and upkeep of intraepithelial T cells 7	*Skint7*
Membrane metallo-endopeptidase-like 1	*Mmel1*		

As the immune checkpoint pathways are major targets in cancer immunotherapy, we further examined expression differences of these pathway components at both RNA and protein levels. Contrary to Pparg expression, T-cells co-stimulatory factors such as cluster of differentiation 80 and 86 (Cd80 and Cd86) were not differentially expressed between strains at either the transcriptional (Figure S2) or protein (**Figure 4B**) levels. Nonetheless, our Western blot results and associated densitometry show significantly increased expression of T-cells inhibitory factor such as the program cell death ligand-1, Pdl-1 (Cd274), in FVB mice relative to C57BL/6 following BBN treatment (p-value = 0.0286, Wilcoxon rank sum test; **Figure 4C**). Interestingly, these differences were less pronounced when the expression of Cd274 in BBN exposed bladders of both strains were compared with unexposed bladders (Figure S3). Our results indicate a BBN-induced activation of immune response signatures in both strain of mice following BBN exposure, with FVB strain exhibiting relatively high levels of inflamed and immunogenic markers.

Discussion

Genetically engineered mouse models are often created through breeding strategies that incorporate various strains. While this approach can be entirely appropriate if genetically similar/identical littermates are used as controls, the association between background strain and carcinogen susceptibility is well documented throughout the field of cancer research [13, 21, 22, 25, 26]. To the best of our knowledge, no study has directly compared the impact of BBN exposure on bladder cancer susceptibility and phenotype between C57BL/6 and FVB, two commonly utilized mouse strains for the study of bladder cancer [40-42]. In this study, we showed that FVB mice are more susceptible to BBN and develop MIBC at just 12 weeks of BBN exposure (**Figure 1**). The BBN-induced tumors in FVB mice were poorly differentiated and morphologically heterogeneous mimicking some features of specific types of human MIBC including conventional UCC, UCC with SqD and UCC with GD (**Figure 2**). On the other hand, following 12 weeks of BBN administration, C57BL/6 mice develop NMIBC characterized by CIS and papillary tumors. However, C57BL/6 mice treated with BBN for 20 weeks develop MIBC with elements of SqD in accordance with previous studies [21, 43]. Both mouse strains exhibited increased expression of basal markers Krt5 and Krt14 (**Figure 3**). In addition, we showed that the FVB tumor microenvironment is highly immunogenic and inflamed with increased expression of murine MHC, immune checkpoint Pdl-1 and pro-inflammatory cytokines (Il-5 and Il-17b) and their respective receptors (Il-5ra, Il-5rb, Il-17ra and Il-17rb) as shown in **Figure 4**.

While adenocarcinoma accounts for 0.5-2% of bladder cancer in the United States [44], mixed GD is the second most common morphologic subtype in cystectomy samples, and both are associated with worse clinical outcome in bladder cancer patients [45, 46]. Although current

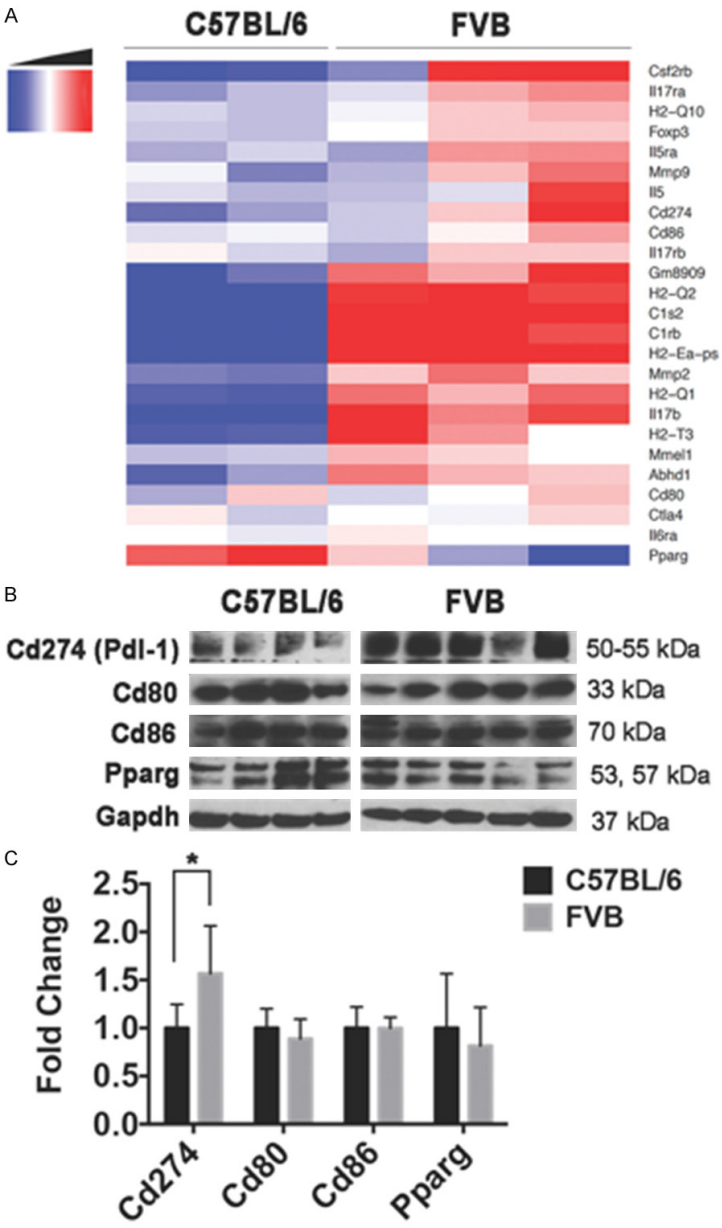

Figure 4. BBN-induced bladder tumors in FVB mice exhibit an inflamed microenvironment and increased expression of Cd274 (Pdl-1). Both C57BL/6 and FVB mice were exposed to BBN for 12 weeks and sacrificed. Following RNA extraction, we performed RNA-seq and Gene Ontology (GO) analysis, which indicated differences in the tumor microenvironment between the two strains. A. Heatmap display of immune-related genes differentially expressed in C57BL/6 and FVB mice at 12 weeks of BBN treatment and identified by GO analysis. FPKM-based gene expression measurements are median centered by row with genes listed in rows and samples (C57BL/6 n = 2; FVB n = 3) in columns. B. Western blot of the immune checkpoints (Cd274/Pdl-1, Cd80 and Cd86), Pparg and Gapdh loading control. Each lane represents one bladder/mouse (C57BL/6 n = 4; FVB n = 5). C. Densitometry analysis of Western blot confirmed significantly higher expression of Cd274/Pdl-1 in FVB than C57BL/6. One FVB mouse outlier (lane 4) was omitted from the densitometry analysis for statistical analysis (*p-value = 0.0286; Wilcoxon rank sum test).

National Comprehensive Cancer Network guidelines indicate that UCC with GD should be treated similarly to conventional UCC [47], proven and effective therapeutic options for adenocarcinoma are limited and under-studied. Therefore, the development of mouse models that exhibit a rapid development of histologic variants such as UCC with GD and adenocarcinoma is crucial for the identification of novel and appropriate therapies. While GD has been previously reported following the exposure of mice on a mixed background to BBN [25], we believe this is the first report describing the presence of GD in FVB mice. As the incidence of GD in the FVB mice increases with prolonged exposure to BBN, this implies that the urothelial tissue may initially develop as UCC with GD, and then progresses in this spectrum to adenocarcinoma upon continuous carcinogen exposure. Bladder adenocarcinoma is often associated with the formation of enteric/mucinous-type glands, and the caudal type homeobox 2 (CDX2) [48] is a marker utilized for assessment of GD. Surprisingly, we failed to detect Cdx2 in all mouse bladder tumors exhibiting any degree of GD suggesting a non-enteric route of gland development in these tumors. Similarly, Pparg expression, which is often associated with urothelial and glandular differentiation was observed to be also lower in the FVB tumors with GD as opposed to the C57BL/6 tumors.

Because human advanced bladder cancer has been associated with the presence of PDL-1 and has proven to be responsive to immune checkpoints blockade [49, 50], our results concerning Cd274/Pdl-1 are significant because of the lack of preclinical

models for the study of immune checkpoint blockade in bladder cancer. This is important because while the development of FDA approved PDL1/PD1 immune checkpoint inhibitors, including Nivolumab, Atezolizumab, Durvalumab and Avelumab, has revolutionized bladder cancer treatment and other malignancies, only a small fraction of patients benefit from these therapies, and PDL-1 detection is not always the best predictor of response. Thus, preclinical models and additional research are needed to identify ways of enhancing immune checkpoint blockade. Our differential expression analysis showed increased levels of Cd274/Pdl-1 expression in FVB than in C57BL/6 after BNN exposure. However, Western blot analysis of BBN exposed bladders of both C57BL/6, and FVB mice showed increased levels of Cd274/Pdl-1 expression when compared with non-exposed bladders. This result suggests that, in addition to genetic background differences, the increase in Cd274/Pdl-1 expression may be due to BBN-associated immunogenic response, and therefore, warrant further investigations.

One limitation of our model is that FVB mice become moribund at 16 weeks of BBN exposure precluding further experimentation to characterize the natural history of glandular changes better. Therefore, future approaches might "rescue" bladder tissue from BBN-treated FVB mice, followed by sub-capsular renal engraftment. This approach would enable investigators to "age" cancerous bladder tissue in a syngeneic host enabling further characterization. This approach could potentially be useful for metastatic disease studies when the tissue is orthotopically implanted in the bladder. In addition, reduced concentrations of BBN could be employed, and it would be advantageous to create cell lines from BBN-induced FVB bladder tumors that retain elements of GD or adenocarcinoma. An additional limitation of this study is that we did not control for BBN consumption between the strains, which could influence tumor development. Moreover, because the RNA-seq analysis was performed solely on carcinogen exposed bladders, the differences in gene expression are assumed to be associated with strain response to BBN exposure; however, these differences could potentially also be baseline differences between the two strains. In that regard, it is noteworthy to highlight that C57BL/6 strain was previously reported to be less immunogenic than, for instance, BABL/C strain in a mouse modeling of human immune thrombocytopenia (ITP) [51]. Although the low levels of inflammatory response in C57BL/6 in the ITP model support our observations that C57BL/6 strain is less immunogenic compared with FVB strain, further studies are warranted to confirm whether the differences in gene expression are driven by intrinsic strain response to carcinogen exposure or are baseline differences of these strains.

In conclusion, we show that FVB strain is more susceptible to BBN and develops advanced bladder cancer at earlier time point than C57BL/6. We also identify important differences between the tumor microenvironments of these two strains in terms of immune signatures following BBN exposure. The increased presence of Cd274/Pdl-1 in the FVB tumor microenvironment indicates that FVB strain can potentially be used as a model for a more in-depth characterization of (1) the interaction between immune cells and tumor cells in advanced stage tumor microenvironment and (2) the impact of histological variants on immunotherapy. Also, based on the degree to which FVB mice rapidly develop bladder cancer with unique histologic attributes following BBN exposure, the current study indicates that investigators should carefully design and interpret their research findings when utilizing genetically engineered mouse models with mixed genetic backgrounds in combination with BBN in an effort to maintain experimental rigor and enhance reproducibility.

Acknowledgements

This project was supported by the National Cancer Institute (R00CA172122; DJD) and the Ken and Bonnie Shockey Fund for Urologic Research (JDR). This work was additionally funded in part by a Medical Student Fellowship (RGO) from the Leo and Anne Albert Institute for Bladder Cancer Care and Research.

Disclosure of conflict of interest

None.

Address correspondence to: Dr. David J DeGraff, Department of Pathology and Laboratory Medicine, Pennsylvania State University College of Medicine, 500 University Drive, Hershey, PA 17033, USA. Tel: 717-531-0003 Ext. 281295; E-mail: ddegraff@pennstatehealth.psu.edu

References

[1] Siegel RL, Miller KD and Jemal A. Cancer statistics, 2018. CA Cancer J Clin 2018; 68: 7-30.

[2] Liebert M, Seigne J. Characteristics of invasive bladder cancers: histological and molecular markers. Semin Urol Oncol 1996; 14: 62-72.

[3] Chalasani V, Chin JL, Izawa JI. Histologic variants of urothelial bladder cancer and nonurothelial histology in bladder cancer. Can Urol Assoc J 2009; 3: S193-8.

[4] Al-Ahmadie HA, Iyer G, Lee BH, Scott SN, Mehra R, Bagrodia A, Jordan EJ, Gao SP, Ramirez R, Cha EK, Desai NB, Zabor EC, Ostrovnaya I, Gopalan A, Chen YB, Fine SW, Tickoo SK, Gandhi A, Hreiki J, Viale A, Arcila ME, Dalbagni G, Rosenberg JE, Bochner BH, Bajorin DF, Berger MF, Reuter VE, Taylor BS, Solit DB. Frequent somatic CDH1 loss-of-function mutations in plasmacytoid variant bladder cancer. Nat Genet 2016; 48: 356-8.

[5] Seiler R, Ashab HAD, Erho N, van Rhijn BWG, Winters B, Douglas J, Van Kessel KE, Fransen van de Putte EE, Sommerlad M, Wang NQ, Choeurng V, Gibb EA, Palmer-Aronsten B, Lam LL, Buerki C, Davicioni E, Sjödahl G, Kardos J, Hoadley KA, Lerner SP, McConkey DJ, Choi W, Kim WY, Kiss B, Thalmann GN, Todenhöfer T, Crabb SJ, North S, Zwarthoff EC, Boormans JL, Wright J, Dall'Era M, van der Heijden MS, Black PC. Impact of molecular subtypes in muscle-invasive bladder cancer on predicting response and survival after neoadjuvant chemotherapy. Eur Urol 2017; 72: 544-554.

[6] Ding J, Xu D, Pan C, Ye M, Kang J, Bai Q, Qi J. Current animal models of bladder cancer: awareness of translatability (Review). Exp Ther Med 2014; 8: 691-9.

[7] Day CP, Merlino G, Van Dyke T. Preclinical mouse cancer models: a maze of opportunities and challenges. Cell 2015; 163: 39-53.

[8] DeGraff DJ, Robinson VL, Shah JB, Brandt WD, Sonpavde G, Kang Y, Liebert M, Wu XR, Taylor JA 3rd; Translational Science Working Group of the BladderAdvocacy Network Think Tank. Current preclinical models for the advancement of translational bladder cancer research. Mol Cancer Ther 2013; 12: 121-30.

[9] Kobayashi T, Owczarek TB, McKiernan JM, Abate-Shen C. Modelling bladder cancer in mice: opportunities and challenges. Nat Rev Cancer 2015; 15: 42-54.

[10] Wu XR. Biology of urothelial tumorigenesis: insights from genetically engineered mice. Cancer Metastasis Rev 2009; 28: 281-90.

[11] Druckrey H, Preussmann R, Ivankovic S, Schmidt C, Mennel H, Stahl K. Selective induction of bladder cancer in rats by DiButyl-and N-Butyl-N-Butanol(4)-Nitrosamine. Z Krebsforsch 1964; 66: 280-90

[12] Bertram JS, Craig AW. Specific induction of bladder cancer in mice by butyl-(4-hydroxybutyl)-nitrosamine and the effects of hormonal modifications on the sex difference in response. Eur J Cancer 1972; 8: 587-94.

[13] Vasconcelos-Nóbrega C, Colaço A, Lopes C, Oliveira PA. Review: BBN as an urothelial carcinogen. In Vivo 2012; 26: 727-39.

[14] Okada M, Suzuki E, Hashimoto Y. Carcinogenicity of N-nitrosamines related to N-butyl-N-(4-hydroxybutyl)nitrosamine and N,N,-dibutylnitrosamine in ACI/N rats. Gan 1976; 67: 825-34.

[15] Suzuki E, Anjo T, Aoki J, Okada M. Species variations in the metabolism of N-butyl-N-(4-hydroxybutyl) nitrosamine and related compounds in relation to urinary bladder carcinogenesis. Gan 1983; 74: 60-8.

[16] Airoldi L, Bonfanti M, Magagnotti C, Fanelli R. Experimental model for investigating bladder carcinogen metabolism using the isolated rat urinary bladder. IARC Sci Publ 1987; 159-61.

[17] He Z, Kosinska W, Zhao ZL, Wu XR, Guttenplan JB. Tissue-specific mutagenesis by N-butyl-N-(4-hydroxybutyl)nitrosamine as the basis for urothelial carcinogenesis. Mutat Res 2012; 742: 92-5.

[18] Hirose M, Fukushima S, Hananouchi M, Shirai T, Ogiso T. Different susceptibilities of the urinary bladder epithelium of animal species to three nitroso compounds. Gan 1976; 67: 175-89.

[19] Shirai T, Murasaki G, Tatematsu M, Tsuda H, Fukushima S. Early surface changes of the urinary bladder epithelium of different animal species induced by N-butyl-N-(4-hydroxybutyl)-nitrosamine. Gan 1977; 68: 203-12.

[20] Suzuki E, Mochizuki M, Okada M. Relationship of urinary N-butyl-N-(3-carboxypropyl)nitrosamine to susceptibility of animals to bladder carcinogenesis by N-butyl-N-(4-hydroxybutyl)nitrosamine. Gan 1983; 74: 360-4.

[21] Ohtani M, Kakizoe T, Sato S, Sugimura T, Fukushima S. Strain differences in mice with invasive bladder carcinomas induced by N-butyl-N-(4-hydroxybutyl)nitrosamine. J Cancer Res Clin Oncol 1986; 112: 107-10.

[22] Akagi G, Akagi A, Kimura M, Otsuka H. Comparison of bladder tumors induced in rats and mice with N-butyl-N-(4-hydroxybutyl)-nitrosoamine. Gan 1973; 64: 331-6.

[23] Bonser G, Clayson D, Jull J. Some aspects of the experimental induction of tumours of the bladder. Br Med Bull 1958; 14: 146-52.

[24] Fukushima S, Hirose M, Tsuda H, Shirai T, Hirao K. Histological classification of urinary bladder cancers in rats induced by N-butyl-n-(4-hydroxybutyl)nitrosamine. Gan 1976; 67: 81-90.

[25] Becci PJ, Thompson HJ, Strum JM, Brown CC, Sporn MB, Moon RC. N-butyl-N-(4-hydroxybutyl) nitrosamine-induced urinary bladder cancer in C57BL/6 X DBA/2 F1 mice as a useful model for study of chemoprevention of cancer with retinoids. Cancer Res 1981; 41: 927-32.

[26] Ohtani M, Kakizoe T, Nishio Y, Sato S, Sugimura T, Fukushima S, Niijima T. Sequential changes of mouse bladder epithelium during induction of invasive carcinomas by N-butyl-N-(4-hydroxybutyl)nitrosamine. Cancer Res 1986; 46: 2001-4.

[27] Benavides F, Gomez G, Venables-Griffith A, Lambertz I, Flores M, Angel JM, Fuchs-Young R, Richie ER, Conti CJ. Differential susceptibility to chemically induced thymic lymphomas in SENCARB and SSIN inbred mice. Mol Carcinog 2006; 45: 543-8.

[28] Maronpot RR. Biological basis of differential susceptibility to hepatocarcinogenesis among mouse strains. J Toxicol Pathol 2009; 22: 11-33.

[29] Reddy OL, Cates JM, Gellert LL, Crist HS, Yang Z, Yamashita H, Taylor JA 3rd, Smith JA Jr, Chang SS, Cookson MS, You C, Barocas DA, Grabowska MM, Ye F, Wu XR, Yi Y, Matusik RJ, Kaestner KH, Clark PE, DeGraff DJ. Loss of FOXA1 drives sexually dimorphic changes in urothelial differentiation and is an independent predictor of poor prognosis in bladder cancer. Am J Pathol 2015; 185: 1385-95.

[30] Ritchie ME, Phipson B, Wu D, Hu Y, Law CW, Shi W, Smyth GK. Limma powers differential expression analyses for RNA-sequencing and microarray studies. Nucleic Acids Res 2015; 43: e47.

[31] Team RC. R: A language and environment for statistical computing. R Foundation for Statistical Computing, Vienna, Austria. http://www.R-project.org., 2018.

[32] Huang da W, Sherman BT, Lempicki RA. Systematic and integrative analysis of large gene lists using DAVID bioinformatics resources. Nat Protoc 2009; 4: 44-57.

[33] Huang da W, Sherman BT, Lempicki RA. Bioinformatics enrichment tools: paths toward the comprehensive functional analysis of large gene lists. Nucleic Acids Res 2009; 37: 1-13.

[34] Nagao M, Suzuki E, Yasuo K, Yahagi T, Seino Y. Mutagenicity of N-butyl-N-(4-hydroxybutyl)nitrosamine, a bladder carcinogen, and related compounds. Cancer Res 1977; 37: 399-407.

[35] Warrick JI, Sjödahl G, Kaag M, Raman JD, Merrill S, Shuman L, Chen G, Walter V, DeGraff DJ. Intratumoral heterogeneity of bladder cancer by molecular subtypes and histologic variants. Eur Urol 2019; 75: 18-22.

[36] Saito R, Smith CC, Utsumi T, Bixby LM, Kardos J, Wobker SE, Stewart KG, Chai S, Manocha U, Byrd KM, Damrauer JS, Williams SE, Vincent BG, Kim WY. Molecular subtype-specific immunocompetent models of high-grade urothelial carcinoma reveal differential neoantigen expression and response to immunotherapy. Cancer Res 2018; 78: 3954-3968.

[37] Robertson AG, Kim J, Al-Ahmadie H, Bellmunt J, Guo G, Cherniack AD, Hinoue T, Laird PW, Hoadley KA, Akbani R, Castro MAA, Gibb EA, Kanchi RS, Gordenin DA, Shukla SA, Sanchez-Vega F, Hansel DE, Czerniak BA, Reuter VE, Su X, de Sa Carvalho B, Chagas VS, Mungall KL, Sadeghi S, Pedamallu CS, Lu Y, Klimczak LJ, Zhang J, Choo C, Ojesina AI, Bullman S, Leraas KM, Lichtenberg TM, Wu CJ, Schultz N, Getz G, Meyerson M, Mills GB, McConkey DJ; TCGA Research Network, Weinstein JN, Kwiatkowski DJ, Lerner SP. Comprehensive molecular characterization of muscle-invasive bladder cancer. Cell 2017; 171: 540-56, e25.

[38] Varley CL, Stahlschmidt J, Smith B, Stower M, Southgate J. Activation of peroxisome proliferator-activated receptor-gamma reverses squamous metaplasia and induces transitional differentiation in normal human urothelial cells. Am J Pathol 2004; 164: 1789-98.

[39] Sweis RF, Spranger S, Bao R, Paner GP, Stadler WM, Steinberg G, Gajewski TF. Molecular drivers of the non-T-cell-Inflamed tumor microenvironment in urothelial bladder cancer. Cancer Immunol Res 2016; 4: 563-8.

[40] Zhang ZT, Pak J, Shapiro E, Sun TT, Wu XR. Urothelium-specific expression of an oncogene in transgenic mice induced the formation of carcinoma in situ and invasive transitional cell carcinoma. Cancer Res 1999; 59: 3512-7.

[41] Lesche R, Groszer M, Gao J, Wang Y, Messing A, Sun H, Liu X, Wu H. Cre/loxP-mediated inactivation of the murine Pten tumor suppressor gene. Genesis 2002; 32: 148-9.

[42] Puzio-Kuter AM, Castillo-Martin M, Kinkade CW, Wang X, Shen TH, Matos T, Shen MM, Cordon-Cardo C, Abate-Shen C. Inactivation of p53 and Pten promotes invasive bladder cancer. Genes Dev 2009; 23: 675-80.

[43] Fantini D, Glaser AP, Rimar KJ, Wang Y, Schipma M, Varghese N, Rademaker A, Behdad A, Yellapa A, Yu Y, Sze CC, Wang L, Zhao Z, Crawford SE, Hu D, Licht JD, Collings CK, Bartom E, Theodorescu D, Shilatifard A, Meeks JJ. A Carcinogen-induced mouse model recapitulates the molecular alterations of human muscle invasive bladder cancer. Oncogene 2018; 37: 1911-1925.

[44] Thomas DG, Ward AM, Williams JL. A study of 52 cases of adenocarcinoma of the bladder. Br J Urol 1971; 43: 4-15.

[45] Rogers CG, Palapattu GS, Shariat SF, Karakiewicz PI, Bastian PJ, Lotan Y, Gupta A,

Vazina A, Gilad A, Sagalowsky AI, Lerner SP, Schoenberg MP. Clinical outcomes following radical cystectomy for primary nontransitional cell carcinoma of the bladder compared to transitional cell carcinoma of the bladder. J Urol 2006; 175: 2048-53; discussion 53.

[46] Mitra AP, Bartsch CC, Bartsch G, Miranda G, Skinner EC, Daneshmand S. Does presence of squamous and glandular differentiation in urothelial carcinoma of the bladder at cystectomy portend poor prognosis? An intensive case-control analysis. Urol Oncol 2014; 32: 117-27.

[47] NCCN Guidelines. National Comprehensive Cancer Network Version 1.2018. Bladder Cancer. https://www.nccn.org/professionals/physician_gls/pdf/bladder.pdf. Accessed January 22, 2018.

[48] Werling RW, Yaziji H, Bacchi CE, Gown AM. CDX2, a highly sensitive and specific marker of adenocarcinomas of intestinal origin: an immunohistochemical survey of 476 primary and metastatic carcinomas. Am J Surg Pathol 2003; 27: 303-10.

[49] Massard C, Gordon MS, Sharma S, Rafii S, Wainberg ZA, Luke J, Curiel TJ, Colon-Otero G, Hamid O, Sanborn RE, O'Donnell PH, Drakaki A, Tan W, Kurland JF, Rebelatto MC, Jin X, Blake-Haskins JA, Gupta A, Segal NH. Safety and efficacy of durvalumab (MEDI4736), an anti-programmed cell death ligand-1 immune checkpoint inhibitor, in patients with advanced urothelial bladder cancer. J Clin Oncol 2016; 34: 3119-25.

[50] Sharma P, Callahan MK, Bono P, Kim J, Spiliopoulou P, Calvo E, Pillai RN, Ott PA, de Braud F, Morse M, Le DT, Jaeger D, Chan E, Harbison C, Lin CS, Tschaika M, Azrilevich A, Rosenberg JE. Nivolumab monotherapy in recurrent metastatic urothelial carcinoma (CheckMate 032): a multicentre, open-label, two-stage, multi-arm, phase 1/2 trial. Lancet Oncol 2016; 17: 1590-8.

[51] Leontyev D, Neschadim A, Branch DR. Cytokine profiles in mouse models of experimental immune thrombocytopenia reveal a lack of inflammation and differences in response to intravenous immunoglobulin depending on the mouse strain. Transfusion 2014; 54: 2871-9.

Table S1. List of genes (n = 75) differentially upregulated (q < 0.05) in FVB versus C57BL/6

C1rb	Gm8615	H2-Ea-ps	Il17b	Kcns1
Serpina1b	Chil1	Gm8909	Gm8580	D030025P21Rik
4933432I03Rik	Gm5801	Xlr3c	H2-Q2	Frmpd3
AA792892	Sorcs3	Mrgprd	Serpina3k	Mup5
Madcam1	Apol11b	Trim34b	Ptprv	C1s2
Cyp4f37	4930565N06Rik	9830107B12Rik	A930015D03Rik	Zfp949
H2-Q1	C920025E04Rik	Eno1b	Gdpd3	Olfr1251
Fam196a	Mir6909	Tekt4	Tpte	C4a
Slc6a3	Zfp605	Cdh16	Gm17746	Mmel1
Gm3558	Tmod4	Mybph	H2-Q10	Ibsp
Hal	Slc24a1	Nlrp5	Dlx4	Gm10653
Slco4c1	H2-T3	Art2a-ps	Abhd1	Al506816
Pcdhb7	Tspan10	Dmp1	Vash2	Snord49b
Ppy	Mir7063	Apom	Dupd1	C330046G13Rik
Tbr1	1700008C04Rik	Scn11a	Tcstv3	Myh7b

Table S2. List of genes (n = 73) differentially downregulated (q < 0.05) in FVB versusC57BL/6

Afm	Gm14305	Mir7688	Fam47e	Mucl1
Gm14393	2310003N18Rik	Olfr1034	Rbmxl2	Gzmk
D730005E14Rik	4930481A15Rik	Tmem181b-ps	Pakap	Actl11
9530027J09Rik	4930505A04Rik	1110019D14Rik	Gm38509	Prr9
Krt33a	Nek11	Wfdc6b	Amer3	Gm16291
8030455M16Rik	Apol10a	Gpr150	Nps	4930546K05Rik
4930479D17Rik	4933427E11Rik	Gm5420	Epha10	Mir687
Sun3	Hist1h2bp	Mirlet7i	4930473A02Rik	Fgf4
Mir6970	C130060K24Rik	Tcaf3	1700125H20Rik	Gipr
Snord85	4930511A02Rik	H2-T23	Skint4	Skint7
Lrrc72	Zcchc13	Ankrd53	Gucy2d	Slc22a22
Prss52	Med9os	Cyp8b1	Sez6	4933433H22Rik
Kcnj13	Ccdc109b	Trim12a	Apoa2	Gabra3
C920006O11Rik	Cda	E130008D07Rik	Ces1f	4930412C18Rik
Cd200r3	Ttc9	Adgb		

Table S3. Clustering of functional annotations enriched in FVB versus C57BL/6 as defined by DAVID analysis of differentially expressed genes (n = 75)

Annotation Cluster 1	Enrichment Score: 3.83	Count	*P*_Value	Benjamini
UP_SEQ_FEATURE	Glycosylation site: N-linked (GlcNAc...)	25	5.70E-07	1.10E-04
UP_SEQ_FEATURE	Signal peptide	21	2.10E-05	9.90E-04
UP_KEYWORDS	Signal	25	3.00E-04	1.70E-02
UP_KEYWORDS	Glycoprotein	22	5.00E-04	1.90E-02
UP_KEYWORDS	Disulfide bond	18	2.40E-03	5.20E-02
UP_SEQ_FEATURE	Disulfide bond	15	2.40E-03	6.30E-02
Annotation Cluster 2	Enrichment Score: 3.63	Count	*P*_Value	Benjamini
INTERPRO	MHC classes I/II-like antigen recognition protein	6	1.20E-06	2.10E-04
KEGG_PATHWAY	Graft-versus-host disease	5	2.40E-06	1.10E-04
GOTERM_BP_DIRECT	Antigen processing and presentation of peptide antigen via MHC class I	5	2.40E-06	4.90E-04
KEGG_PATHWAY	Allograft rejection	5	3.20E-06	7.20E-05
INTERPRO	Immunoglobulin/major histocompatibility complex, conserved site	6	3.40E-06	3.00E-04
KEGG_PATHWAY	Type I diabetes mellitus	5	4.80E-06	7.20E-05
UP_KEYWORDS	MHC I	4	4.90E-06	5.60E-04
GOTERM_MF_DIRECT	Peptide antigen binding	5	6.40E-06	7.40E-04
SMART	IGc1	6	6.60E-06	2.40E-04
INTERPRO	MHC class I, alpha chain, alpha1/alpha2	5	6.70E-06	3.90E-04
INTERPRO	Immunoglobulin C1-set	6	8.00E-06	3.50E-04
KEGG_PATHWAY	Autoimmune thyroid disease	5	8.30E-06	9.30E-05
KEGG_PATHWAY	Cell adhesion molecules (CAMs)	6	9.70E-06	8.70E-05
GOTERM_CC_DIRECT	MHC class I protein complex	4	1.10E-05	7.80E-04
UP_SEQ_FEATURE	Region of interest: Alpha-3	4	1.20E-05	1.10E-03
KEGG_PATHWAY	Viral myocarditis	5	1.30E-05	9.50E-05
KEGG_PATHWAY	Antigen processing and presentation	5	1.50E-05	9.50E-05
UP_SEQ_FEATURE	Region of interest: Alpha-1	4	1.60E-05	1.00E-03
UP_SEQ_FEATURE	Region of interest: Alpha-2	4	1.60E-05	1.00E-03
INTERPRO	MHC class I-like antigen recognition	5	1.90E-05	6.50E-04
UP_SEQ_FEATURE	Domain: Ig-like C1-type	4	9.80E-05	3.70E-03
UP_SEQ_FEATURE	Region of interest: Connecting peptide	4	1.20E-04	3.60E-03
GOTERM_MF_DIRECT	TAP binding	3	2.00E-04	1.10E-02
KEGG_PATHWAY	Phagosome	5	2.80E-04	1.60E-03
GOTERM_MF_DIRECT	Beta-2-microglobulin binding	3	5.40E-04	2.10E-02
KEGG_PATHWAY	Herpes simplex infection	5	5.50E-04	2.80E-03
GOTERM_MF_DIRECT	T cell receptor binding	3	6.30E-04	1.80E-02
UP_KEYWORDS	Immunity	7	6.60E-04	1.80E-02
GOTERM_MF_DIRECT	Receptor binding	7	7.90E-04	1.80E-02
GOTERM_CC_DIRECT	Golgi medial cisterna	3	9.80E-04	1.80E-02
GOTERM_CC_DIRECT	Endoplasmic reticulum exit site	3	1.20E-03	1.80E-02
KEGG_PATHWAY	HTLV-I infection	5	1.60E-03	7.40E-03
INTERPRO	Immunoglobulin-like fold	10	2.70E-03	7.50E-02
INTERPRO	Immunoglobulin-like domain	9	3.30E-03	7.80E-02
KEGG_PATHWAY	Epstein-Barr virus infection	4	7.60E-03	3.10E-02
KEGG_PATHWAY	Viral carcinogenesis	4	9.20E-03	3.40E-02
KEGG_PATHWAY	Endocytosis	4	1.50E-02	5.20E-02
GOTERM_MF_DIRECT	Peptide binding	3	2.60E-02	4.00E-01
GOTERM_MF_DIRECT	Protein heterodimerization activity	4	1.60E-01	8.90E-01
GOTERM_BP_DIRECT	Immune response	3	1.60E-01	1.00E+00
GOTERM_CC_DIRECT	Golgi apparatus	6	2.30E-01	8.80E-01
GOTERM_CC_DIRECT	Cell surface	4	2.50E-01	8.80E-01
GOTERM_CC_DIRECT	Endoplasmic reticulum	6	3.00E-01	8.80E-01
GOTERM_MF_DIRECT	Poly(A) RNA binding	4	5.80E-01	1.00E+00

Annotation Cluster 3	Enrichment Score: 3.48	Count	*P*_Value	Benjamini
UP_SEQ_FEATURE	Signal peptide	21	2.10E-05	9.90E-04
GOTERM_CC_DIRECT	Extracellular region	15	2.00E-04	7.40E-03
GOTERM_CC_DIRECT	Extracellular space	13	6.40E-04	1.60E-02
UP_KEYWORDS	Secreted	12	4.30E-03	7.80E-02
Annotation Cluster 4	Enrichment Score: 0.93	Count	*P*_Value	Benjamini
UP_SEQ_FEATURE	Transmembrane region	19	1.20E-02	2.50E-01
UP_SEQ_FEATURE	Topological domain: Extracellular	12	2.10E-02	3.50E-01
UP_SEQ_FEATURE	Topological domain: Cytoplasmic	13	4.60E-02	5.90E-01
UP_KEYWORDS	Transmembrane helix	24	1.20E-01	8.40E-01
UP_KEYWORDS	Transmembrane	24	1.30E-01	8.20E-01
GOTERM_CC_DIRECT	Integral component of membrane	23	2.30E-01	9.00E-01
UP_KEYWORDS	Membrane	27	2.50E-01	9.50E-01
GOTERM_CC_DIRECT	Plasma membrane	14	6.00E-01	9.90E-01
GOTERM_CC_DIRECT	Membrane	19	6.80E-01	1.00E+00
Annotation Cluster 5	Enrichment Score: 0.6	Count	*P*_Value	Benjamini
UP_SEQ_FEATURE	Active site: Charge relay system	3	9.30E-02	7.80E-01
UP_KEYWORDS	Hydrolase	8	1.40E-01	8.20E-01
GOTERM_MF_DIRECT	Hydrolase activity	7	2.30E-01	9.50E-01
GOTERM_MF_DIRECT	Peptidase activity	3	4.10E-01	1.00E+00
UP_KEYWORDS	Protease	3	4.20E-01	9.90E-01
GOTERM_BP_DIRECT	Proteolysis	3	4.60E-01	1.00E+00
Annotation Cluster 6	Enrichment Score: 0.29	Count	*P*_Value	Benjamini
GOTERM_BP_DIRECT	Ion transport	3	4.60E-01	1.00E+00
UP_KEYWORDS	Ion transport	3	4.90E-01	9.90E-01
GOTERM_BP_DIRECT	Transport	6	5.40E-01	1.00E+00
UP_KEYWORDS	Transport	6	5.70E-01	1.00E+00
Annotation Cluster 7	Enrichment Score: 0.11	Count	*P*_Value	Benjamini
UP_KEYWORDS	Metal-binding	10	5.50E-01	1.00E+00
GOTERM_MF_DIRECT	Metal ion binding	7	9.10E-01	1.00E+00
UP_KEYWORDS	Zinc	4	9.30E-01	1.00E+00
Annotation Cluster 8	Enrichment Score: 0.05	Count	*P*_Value	Benjamini
GOTERM_CC_DIRECT	Intracellular	4	8.30E-01	1.00E+00
UP_KEYWORDS	Zinc	4	9.30E-01	1.00E+00
UP_KEYWORDS	Zinc-finger	3	9.30E-01	1.00E+00

Table S4. Clustering of functional annotations enriched in C57BL/6 versus FVB as defined by DAVID analysis of differentially expressed genes (n=73)

Annotation Cluster 1	Enrichment Score: 1.17	Count	*P*_Value	Benjamini
UP_SEQ_FEATURE	Signal peptide	15	3.00E-04	2.80E-02
UP_SEQ_FEATURE	Domain: Ig-like C1-type	3	1.70E-03	8.10E-02
UP_KEYWORDS	Signal	18	9.40E-03	6.10E-01
UP_SEQ_FEATURE	Topological domain: Extracellular	10	1.10E-02	3.10E-01
UP_SEQ_FEATURE	Transmembrane region	14	2.00E-02	3.30E-01
UP_SEQ_FEATURE	Disulfide bond	10	2.20E-02	3.00E-01
UP_KEYWORDS	Disulfide bond	12	5.80E-02	9.50E-01
GOTERM_CC_DIRECT	Integral component of membrane	19	9.90E-02	1.00E+00
UP_SEQ_FEATURE	Topological domain: Cytoplasmic	9	1.10E-01	8.00E-01
UP_SEQ_FEATURE	Glycosylation site: N-linked (GlcNAc...)	10	1.40E-01	8.50E-01
UP_KEYWORDS	Transmembrane helix	19	1.90E-01	1.00E+00
UP_KEYWORDS	Transmembrane	19	1.90E-01	1.00E+00
UP_KEYWORDS	Alternative splicing	14	2.00E-01	9.70E-01
INTERPRO	Immunoglobulin-like domain	4	2.80E-01	1.00E+00
INTERPRO	Immunoglobulin-like fold	4	3.80E-01	1.00E+00
GOTERM_CC_DIRECT	Membrane	16	4.10E-01	1.00E+00
UP_SEQ_FEATURE	Splice variant	10	4.20E-01	1.00E+00
UP_KEYWORDS	Glycoprotein	10	4.20E-01	1.00E+00
UP_KEYWORDS	Membrane	20	4.80E-01	1.00E+00
Annotation Cluster 2	Enrichment Score: 0.99	Count	*P*_Value	Benjamini
UP_SEQ_FEATURE	Domain: Ig-like V-type	3	1.50E-02	3.00E-01
UP_KEYWORDS	Immunoglobulin domain	3	2.70E-01	9.90E-01
INTERPRO	Immunoglobulin-like domain	4	2.80E-01	1.00E+00
Annotation Cluster 3	Enrichment Score: 0.71	Count	*P*_Value	Benjamini
UP_SEQ_FEATURE	Topological domain: Extracellular	10	1.10E-02	3.10E-01
GOTERM_CC_DIRECT	Plasma membrane	9	7.90E-01	1.00E+00
UP_KEYWORDS	Cell membrane	7	8.30E-01	1.00E+00
Annotation Cluster 4	Enrichment Score: 0.38	Count	*P*_Value	Benjamini
GOTERM_BP_DIRECT	Ion transport	3	3.00E-01	1.00E+00
UP_KEYWORDS	Ion transport	3	3.80E-01	1.00E+00
GOTERM_BP_DIRECT	Transport	5	4.50E-01	1.00E+00
UP_KEYWORDS	Transport	5	5.80E-01	1.00E+00
Annotation Cluster 5	Enrichment Score: 0.3	Count	*P*_Value	Benjamini
INTERPRO	Protein kinase, catalytic domain	3	2.70E-01	1.00E+00
INTERPRO	Protein kinase-like domain	3	3.00E-01	1.00E+00
GOTERM_MF_DIRECT	Protein kinase activity	3	3.10E-01	1.00E+00
GOTERM_MF_DIRECT	Nucleotide binding	4	7.90E-01	1.00E+00
GOTERM_MF_DIRECT	ATP binding	3	8.40E-01	1.00E+00
UP_KEYWORDS	Nucleotide-binding	3	8.90E-01	1.00E+00
Annotation Cluster 6	Enrichment Score: 0.14	Count	*P*_Value	Benjamini
GOTERM_CC_DIRECT	Intracellular	5	3.90E-01	1.00E+00
UP_KEYWORDS	Zinc	4	8.30E-01	1.00E+00
UP_KEYWORDS	Zinc-finger	3	8.50E-01	1.00E+00
UP_KEYWORDS	Metal-binding	6	8.60E-01	1.00E+00
GOTERM_MF_DIRECT	Metal ion binding	6	8.70E-01	1.00E+00

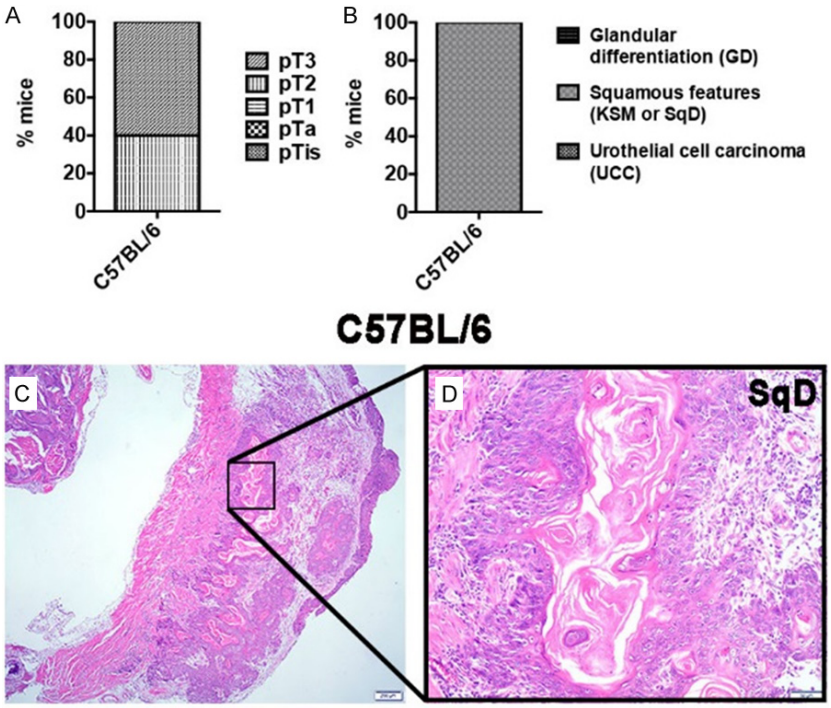

Figure S1. C57BL/6 Mice Develop Advanced Bladder Cancer with Squamous Morphologic Variants upon 20 Weeks of BBN. A. Quantification ofpercentage of C57BL/6 (n = 5) mice at different tumor stages pT2 (n = 2) and pT3 (n = 3) at 20 weeks of BBN exposure. B. Percentage of C57BL/6 (n = 5) mice per morphologic variant at 20 weeks of BBN exposure: all mice developed squamous elements. C. H&E of C57BL/6 bladders showing invasive UCC admixed with SqD in the presence of intracellular bridging and keratin deposition. D. Inset of C showing squamous differentiation.

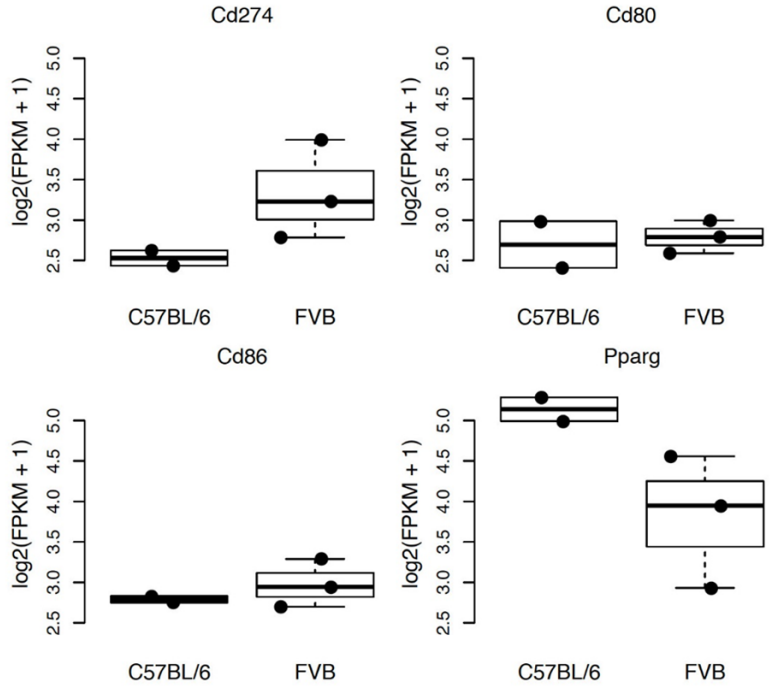

Figure S2. BBN-Induced Bladder Tumors in FVB Mice Exhibit an Increased Level of Transcripts of Cd274 (Pdl-1). Boxplot analysis of absolute expression of transcript levels of Cd274/Pdl-1, Cd80, Cd86 and Pparg in C57BL/6 and FVB bladders exposed to BBN for 12 weeks. Each dot represents one animal.

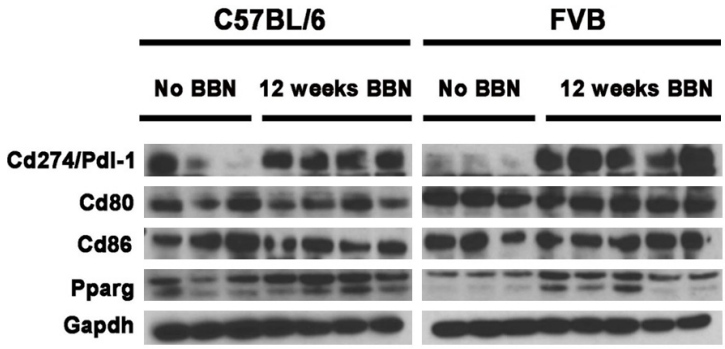

Figure S3. BBN Induces Inflammatory Response in C57BL/6 and FVB Mice. Western blot of the immune checkpoints (Cd274/Pdl-1, Cd80 and Cd86), Pparg, and Gapdh loading control in normal urothelium (no BBN) versus tumors (12 weeks BBN) in C57BL/6 and FVB mice. Each lane represents one bladder: C57BL/6 no BBN (n = 3) and 12 weeks BBN (n = 4); and FVB no BBN (n = 3) and 12 weeks BBN (n = 5).